Temperature, Oxygen, and Soot-Volume-Fraction Measurements in a Turbulent C_2H_4-Fueled Jet Flame

Sean P. Kearney, Daniel R. Guildenbecher, Caroline Winters, Thomas W. Grasser, Paul A. Farias, and John C. Hewson

Sandia National Laboratories

Temperature, Oxygen, and Soot-Volume-Fraction Measurements in a Turbulent C_2H_4-Fueled Jet Flame

Sean P. Kearney, Daniel R. Guildenbecher, Caroline Winters, Paul A. Farias,
and Thomas W. Grasser
Diagnostic Science and Engineering Department, 1512

John C. Hewson
Fire Science and Technology Department, 1532

Sandia National Laboratories
P.O. Box 5800
Albuquerque, New Mexico 87185

Abstract

We present a detailed set of measurements from a piloted, sooting, turbulent C_2H_4-fueled diffusion flame. Hybrid femtosecond/picosecond coherent anti-Stokes Raman scattering (CARS) is used to monitor temperature and oxygen, while laser-induced incandescence (LII) is applied for imaging of the soot volume fraction in the challenging jet-flame environment at Reynolds number, Re = 20,000. Single-laser shot results are used to map the mean and rms statistics, as well as probability densities. LII data from the soot-growth region of the flame are used to benchmark the soot source term for one-dimensional turbulence (ODT) modeling of this turbulent flame. The ODT code is then used to predict temperature and oxygen fluctuations higher in the soot oxidation region higher in the flame.

CONTENTS

(this page has been intentionally left blank)

FIGURES

NOMENCLATURE

b	subscript indicating blackbody conditions
CARS	coherent anti-Stokes Raman scattering
D	diameter of the main fuel jet tube (3.2 mm)
f_v	soot volume fraction
I	Radiation intensity
LII	laser-induced incandescence
r	radial coordinate
s	spatial coordinate
SLPM	standard liters per minute
T	temperature
z	vertical height above the burner exit
μ	extinction coefficient
λ	wavelength

1. INTRODUCTION

Radiative heat transfer from fires and sooting flames in general is dominated by emission and absorption from soot, making accurate soot modeling essential for practical risk analysis. Radiative heat transfer from sooting flames is generated in high-temperature regions by emission from hot soot. In lower temperature regions, soot can act as an absorber, providing shielding of the surroundings from flame radiation. These effects are captured in heat-transfer calculations for fire risk assessment through the radiative transfer equation (RTE),

$$\frac{d\overline{I_\lambda}}{ds} = \overline{\mu_\lambda I_{\lambda,b}}(T) - \overline{\mu_\lambda I_\lambda} \qquad . \tag{1}$$

In Eq. 1, the subscript λ indicates the optical wavelength, while b indicates blackbody conditions at the local temperature, T; I is the radiation intensity, μ is the absorption coefficient and s is a spatial coordinate. Eq. 1 is a simple statement that the change in radiation intensity along a line-of-sight path is equal to emission minus absorption (when scattering is neglected). Emission is represented by the first term on the right-hand side of Eq. 1, while absorption is indicated by the second term.

Reliable, experimentally validated evaluation of Eq. 1 is a requirement for accurate fire risk assessment modeling and requires knowledge of both the temperature and the soot concentration (through μ_λ) fields, which also must be adequately predicted. Soot is a particularly vexing part of fire radiation problem. Soot formation remains a topic of considerable debate, and soot transport is complicated because its diffusion is slow relative to other scalar quantities and, therefore, is not well-scaled by the mixture fraction [1]. Because of these complications, experimental measurements of both the soot concentration and the local temperature in realistic turbulent flames are needed. Measurement of these two "pieces of the fire radiation puzzle" should have high spatial resolution to resolve the highly strained soot containing regions as well as adequate temporal resolution to capture turbulent fluctuations.

Sooting, turbulent environments present significant challenges to any measurement campaign. Physical sensors, such as thermocouples and extractive sampling probes, are invasive, readily clog or coat with soot, suffer from both radiative and conductive bias errors, and can exhibit limited time resolution due to probe thermal inertia [2]. Laser and optical diagnostics can overcome these disadvantages, but are additionally challenged by optical background arising from soot luminosity, scattering and absorption, and by heat transfer to the optical setups. Nevertheless, optical techniques have been successfully applied to sooting turbulent flames for spatially and temporally resolved measurements [3, 4], and have recently been applied to meter-scale turbulent pool fires for temperature and soot field evaluation [5-8] at the Sandia FLAME facility.

In this work, we present measurements of the temperature and soot fields in a turbulent ethylene-fueled jet flamer under laboratory conditions. This flame represents a canonical geometry that is amenable to soot radiation modeling, and permits us to acquire much larger data records needed to generate the statistical quantities in Eq. 1 than would typically be possible in large test facilities like FLAME, with lower cost and higher fidelity. Flame temperatures are measured

using ultrafast coherent anti-Stokes Raman scattering (CARS), which additionally provides information on oxygen content and potentially some product species. The addition of ultrafast laser pulses to the CARS technique also permits us to sample at a data rate that is 100× faster than in [5], with significant reduction in measurement uncertainty. Soot volume concentration is imaged using laser-induced incandescence (LII). The soot measurements are used to benchmark soot-production terms in one dimensional turbulence (ODT) simulations which are being conducted simultaneously [1].

2. EXPERIMENTAL FACILITIES

1.1 Piloted Jet Flame Burner

A piloted, turbulent C_2H_4 jet flame at Reynolds number $Re = 20{,}000$ is established using the piloted burner design described in detail by Zhang *et al.* [9]. Digital photographs of the burner are shown in Figure 1. A $D = 3.2$-mm main-jet fuel tube is centered in a 15.2-mm inner-diameter stainless steel tube which contains the premixed pilot flame gases. The annular space formed by the inner fuel jet and the outer pilot flame assembly is capped with a perforated plate, upon which a lean premixed pilot flame is stabilized. The pilot and main jet tubes are surrounded by a conditioned coflow air assembly, which is 152-mm × 152-mm square. The main fuel jet is pure C_2H_4 at a flow rate of 26.2 SLPM, and the pilot-flame gas flows are 0.53 SLPM of C_2H_4 and 8.4 SLPM of air. Coflow air is supplied at 1500 SLPM, which results in a coflow velocity of 1.07 m/s at the burner face. Short- and long-exposure photographs of the resulting jet flame are shown in Figure 2. The visible flame height indicated by soot luminosity is ~850-900 mm. The soot distribution in this flame has been mapped via planar LII by Shaddix *et al.* [10], who report peak soot volume fractions of $f_v \sim 0.5$-0.6 ppm along the flame centerline. This degree of soot loading presents a significant challenge for many laser-diagnostic approaches due to high levels of soot absorption and scattering, background luminosity and heat flux to the surrounding optics.
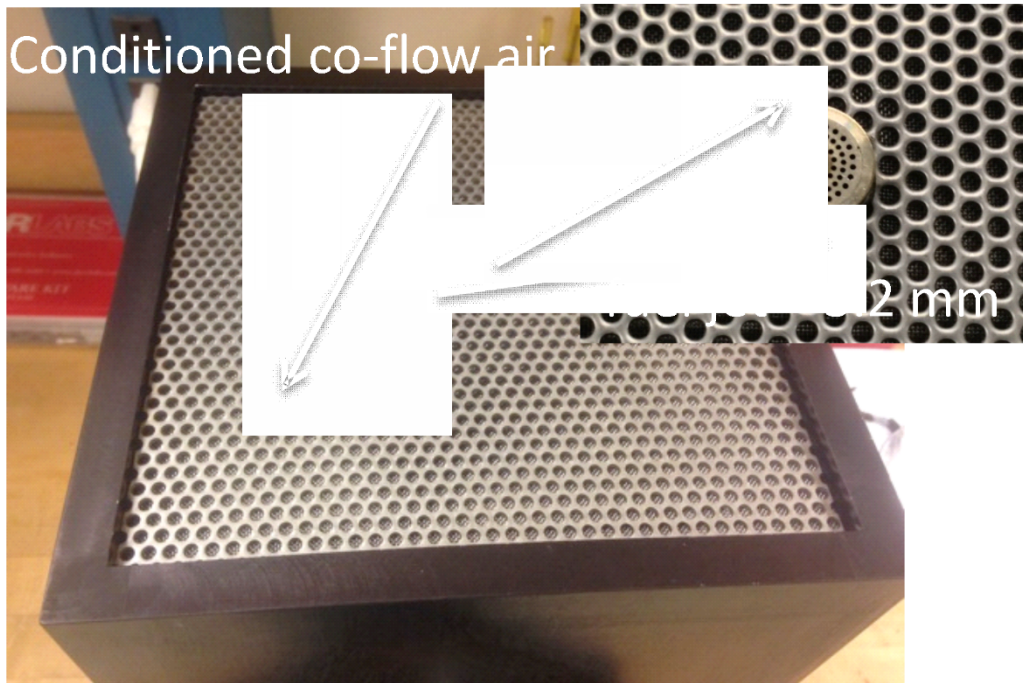

Figure 1. Piloted jet flame burner constructed based on design of Zhang et al. [1].
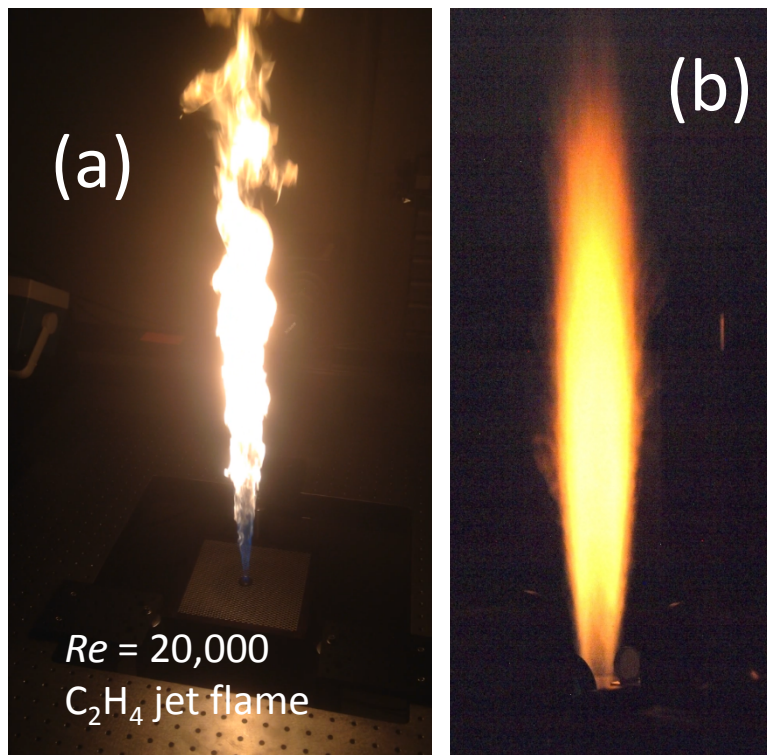
Figure 2. Digital photographs of the Re = 20,000 C₂H₄ jet flame. A short-exposure is shown in (a), while a long-time average is shown in (b).

2.2 Coherent Anti-Stokes Raman Scattering Instrumentation

At present, we have acquired pure-rotational CARS measurements of temperature and relative oxygen content within the region of peak soot loading and into the soot oxidation region, specifically for z/D = 127-175. The hybrid, pure-rotational CARS scheme used for the jet-flame measurements is described in detail in [11] and is briefly summarized here. A schematic of the CARS optical setup is provided in Figure 3. A rotational Raman coherence is prepared by 100-fs-duration pump and Stokes laser pulses (shown in red) whose spectra are centered at 803 nm, with 190 cm^{-1} bandwidth, and pulse energies of ~100 μJ/pulse. A 400-nm, 5-ps-duration probe pulse (shown in blue) is phase-locked to the pump/Stokes preparation and introduced at a delay of τ = 16 ps to generate the CARS signal. The high-energy, 800-1000 μJ, probe pulse is generated using second-harmonic bandwidth compression [11] to convert broadband 100-fs pump pulses to frequency narrow probe radiation with a bandwidth of 3.5 cm^{-1}. A 500-mm focal length beam-crossing lens focuses the pump, Stokes and probe beams in a planar BOXCARS [12] configuration. The resulting CARS measurement volume is ellipsoidal and is ~100 μm in diameter with 90% of the CARS signal generated in a 1.8-mm axial length.

The resulting CARS signal is monitored at 1 kHz using a dual-channel detection system that optimizes the dynamic range of the temperature measurements. Enhanced dynamic range is required in turbulent flames, where the local temperature can vary from near room temperature to over 2000 K on a shot-to-shot basis. Over this temperature range, CARS signal strengths can vary by a factor of several hundred to a thousand, so that the dynamic range of a single detector is not sufficient to capture the full span of thermal conditions. Approximately 4% of the total CARS signal is split using a 3-degree uncoated glass wedge and sent to the "cold-channel" detection system, while 96% of the total signal is transmitted through the wedge to the "hot-channel" detector for the bulk of the combustion gas measurements. The "hot channel" is composed of a 1-m spectrograph with an 1800 l/mm grating that is coupled to a backside-illuminated electron-multiplying CCD (Andor Newton) detector, with 16-bit dynamic range. The "cold channel" is constructed from a lower-resolution 0.33-m spectrometer coupled to a second electron-multiplying CCD (Andor iXon), digitized at over 15 bits. Electron-multiplication gain was not applied in these measurements. Sensitivity of the hot channel detection is optimized for detection of low CARS signals from high-temperature combustion gases by a 2× binning of the horizontal pixels in conjunction with high detector gain setting of ~1e$^-$/count. Cold-channel sensitivity is tuned for significantly larger CARS signals by using neutral density filters and a reduced detector gain of as little as 17 e$^-$/count to avoid saturation that results from high peak signals from cold gas transported into the measurement volume. The dispersion of the two channels is ~0.96 and ~0.71 cm^{-1}/pixel, for hot and cold detection, respectively, while the resolving power of the hot-channel detection is ~3× greater that of the cold.

CARS spectra are recorded at 1-kHz data rate with 10,000 laser shots (10-second duration samples) acquired at each spatial location. Single-laser-shot spectra are accepted as valid when peak counts are below saturation while remaining above a threshold level of 500 peak detector counts. Typical valid shot counts were 95-99% for the combined data yield of both hot and cold channels at each spatial location.
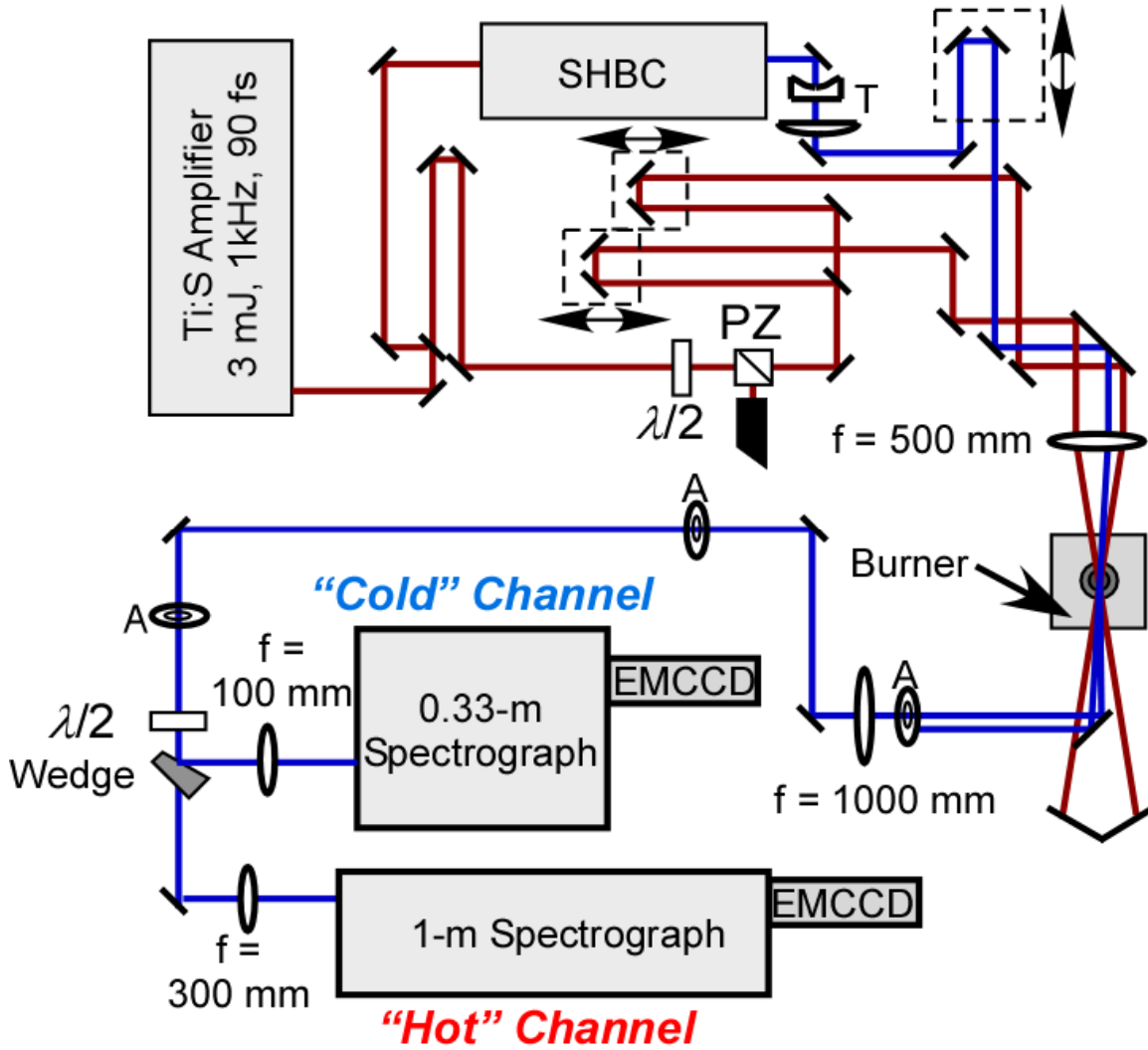
Figure 3. Schematic of CARS instrument for temperature and oxygen measurements: f = lens focal length; $\lambda/2$ = half wave plate; A = aperture; T = telescope; SHBC = second-harmonic bandwidth compressor.

Ensembles of several hundred thousand single-laser-shot CARS spectra were acquired from the turbulent flame in order to obtain well-converged temperature and oxygen statistics. The spectra were fit to a theoretical spectral model using a parallelized Matlab cluster. Uncertainty in the temperature and oxygen measurements was assessed in stable premixed C_2H_4/air and H_2/air flames [11]. Temperature measurement accuracy was generally 3-5%, while the accuracy of the O_2/N_2 ratio was 5-10% when O_2/N_2 was greater than ~6%. At lower O_2/N_2, measurement accuracy degrades as the single-shot detection limit of a few percent O_2/N_2 is approached. The precision of the measured temperatures was 1-2% when the signal exceeded ~1600 detector counts, degrading to roughly 6% for the threshold level of 500 counts. Precision in the O_2/N_2 ratio was 2% or better for similar range of CARS signal strengths, and degraded to ~15% as the 500-count threshold limit was approached.

2.3 Laser-Induced Incandescence Instrument

A schematic of the laser-induced incandescence (LII) instrument used for soot-volume-fraction imaging is shown in Figure 4. A Q-switched Nd:YAG laser provided 800 mJ pulses of ~8-ns duration at a repetition rate of 10 Hz and a wavelength of 1064 nm. A combination of cylindrical and spherical lenses was used to create a thin sheet of laser light, which was ~30 mm in height along the streamwise direction of the jet flame gases, with a focused beam waist near 100 μm achieved along the centerline of the flame. Laser radiation is readily absorbed by soot, which is subsequently heated to temperatures that can approach the soot vaporization point in excess of 4000 K [13]. As a result of the nonlinear $T^4 - T^5$ scaling[†] of soot thermal radiation, the laser-heated soot emits thermally at levels that overwhelm the luminosity from nascent soot at much lower flame temperatures near 1400-1800 K. An intensified CCD camera is used to image the incandescent thermal emission using a narrow 30-ns gate (exposure), which is timed promptly with the arrival of the LII laser pulse. For nanometer-sized soot primary particles, the incandescent soot emission is nearly proportional to the volume of the emitting soot aggregates [13], so that the LII signal is essentially proportional to the local soot volume fraction, f_v, in the flame, thereby constituting a soot volume concentration diagnostic.

The Nd:YAG laser fluence high enough to operate in the so-called plateau-level [7, 13] regime, where the LII signal is largely insensitive to absorption of the interrogating laser beam at it propagates to the measurement volume at the center of the flame. Soot LII images were calibrated against laser light extinction measurements in a laminar C_2H_4 diffusion flame using the approach described by Frederickson *et al.* [7]. Using this procedure, the accuracy of the soot-volume-fraction data is estimated to be 23%, which primarily results from uncertainties in literature values of the soot refractive index and from the uncertainty in the light-extinction data used for calibration.
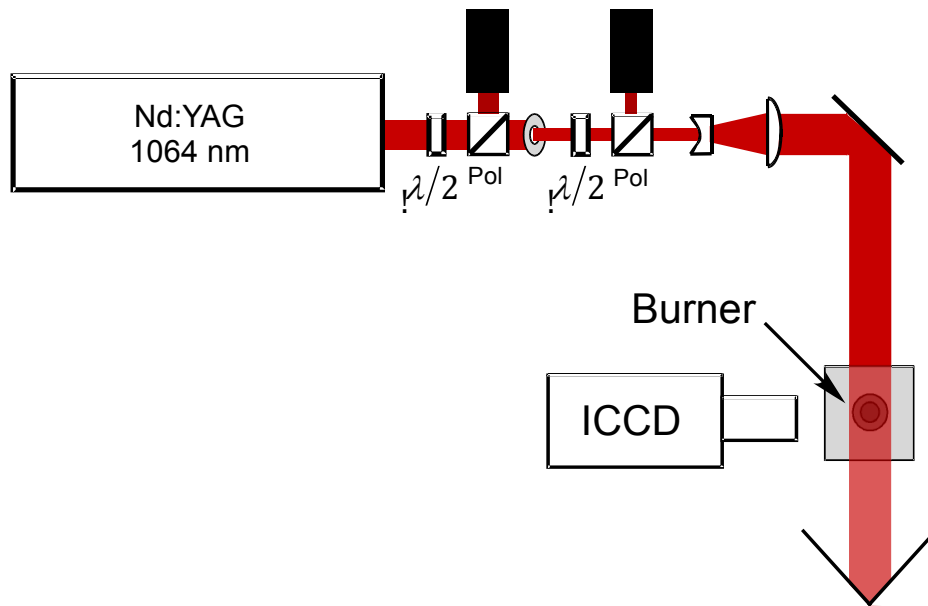

Figure 4. Schematic of LII instrument for soot-volume-fraction measurements: $\lambda/2$ = half wave plate; pol = polarizer; ICCD = intensified CCD camera.

[†] Soot emissivity can scale linearly with T compounding the usual T^4 scaling of thermal radiation to as high as T^5.

(this page has been intentionally left blank)

3. RESULTS AND DISCUSSION

Single-laser-shot LII images of soot volume fraction are shown in Figure 5. The images represent an essentially instantaneous (30-ns resolution) snapshot of the instantaneous structure of the soot field in this highly turbulent flame over a field of view that is ~29 mm (9.1D) per side. The spatial resolution in these soot measurements is ~60 μm with an out-of-plane resolution that is dictated by the laser sheet thickness, ranging from ~100 μm at the center of the images, where the laser sheet is most tightly focused, to about 300 μm at the lateral edges of the images where $x/D = \pm 4$. At this level of spatial resolution, the structure of the highly strained soot structures, which can be submillimeter, is well resolved. These LII images were recorded at a height of $z/D = 103 – 112$ above the burner, a region of the flame that earlier measurements by Shaddix *et al.* [10] reveal to be primarily described by soot growth.

LII images were taken with the field of view centered at three additional heights in the soot growth region, at $z/D = 77, 87, 97$ in addition to 107 in Figure 5. Probability densities (pdf) the turbulent soot-volume-fraction fluctuations could then be generated by binning the LII realizations from all pixels and for all of the 500 single-laser-shot images acquired at each height above the burner. These pdf data are shown in Figure 6, where the LII-measured results are shown as dashed lines with predicted soot pdf results from one-dimensional turbulence (ODT) modeling [1] shown as solid curves. The source term in the ODT model was calibrated to obtain the best possible agreement with the mean soot f_v measured by LII. Measured and predicted soot pdf results are qualitatively similar, but with some distinct quantitative differences. The LII-measured pdf data display distinct maxima away from zero, which move toward larger soot f_v with increasing height in the flame, as one might expect in this range of z/D where soot growth dominates. These maxima are all below 0.1 ppm in this region. In contrast, the modeled pdf results consistently display a most probable soot concentration at zero, with secondary maxima which exceed the values in the measured pdf data, increasing from ~0.1 to 0.25 ppm as z/D increases from 87-107.

CARS temperature measurements were performed higher in the flame at $z/D = 130 – 175$, where the temperatures predicted by ODT with the soot source term calibrated lower in the flame can be compared to the experiment. Single-laser-shot fs/ps rotational CARS spectra obtained at the radial centerline of the jet flame at a height of $z/D = 175$ are shown in Figure 7. This location is within the soot oxidation/overfire region, where the Shaddix *et al.* LII measurements [10] indicate a mean soot volume fraction near 0.3 ppm. Similar quality spectra were obtained lower in the flame, in the region where soot loading peaks near $f_v = 0.5$−0.6 ppm—a peak soot loading that results in the most stringent test for the CARS diagnostic. The spectra are free of nonresonant background in this heavily sooting hydrocarbon rich flame, and are well fit by the theoretical CARS spectral model [11]. Spectra on the left-hand side of the Figure 7(a,b) were obtained from the hot-channel detector, while the results on the right-hand side have been obtained on the cold-channel under conditions where the hot-channel detector is saturated. Between the spectrum in Figure 7d, at $T = 585$ K, and the spectrum in Figure 7a, fitted to $T = 1885$ K, the expected CARS signal strength changes by a factor of 160, illustrating the enhanced dynamic range offered by the two-channel CARS detection system.
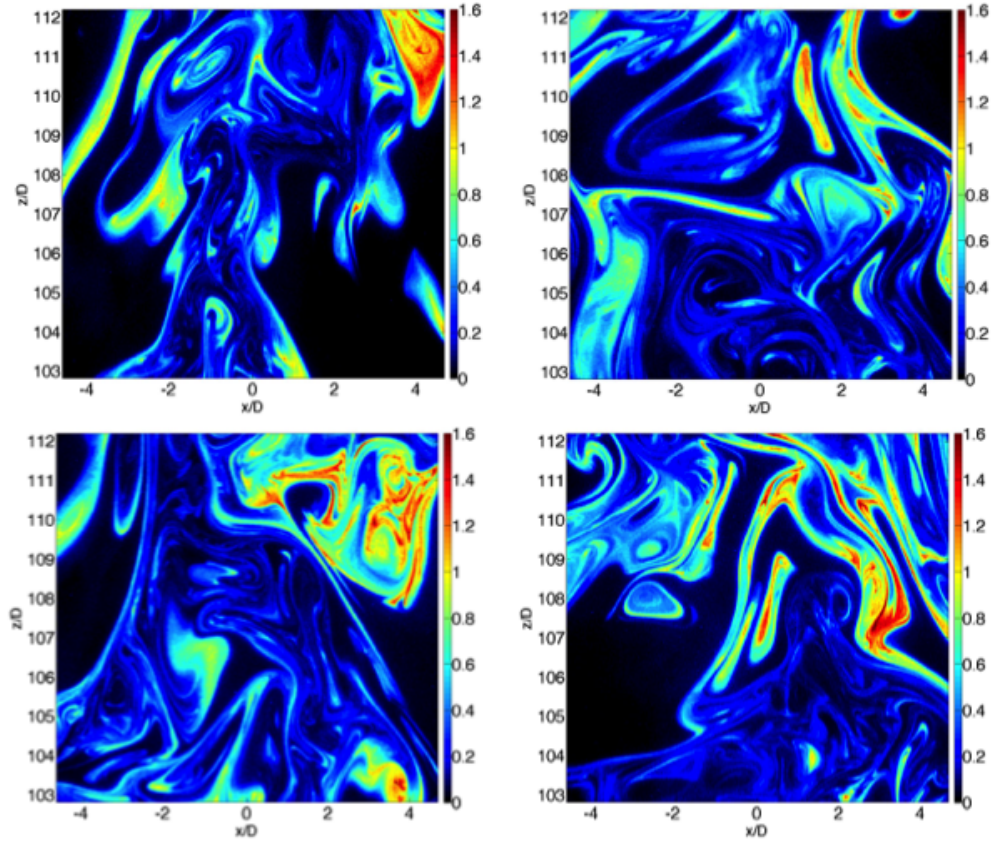
Figure 5. Single-laser-shot soot-volume-fraction images at *z/D* = 107. The color scale represents soot volume fraction in ppm.
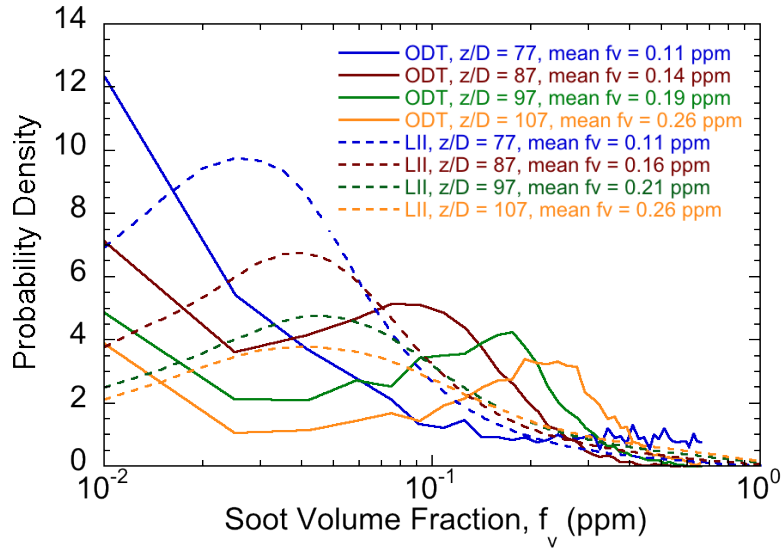

Figure 6. Probability densities of the turbulent soot-volume-fraction fluctuations in the soot-growth region: LII measurements are shown as dashed lines, while ODT simulations are shown as solid curves. Vertical z/D location is color coded.

18

Ensembles of single-laser-shot CARS spectra have been obtained on a grid of spatial locations throughout the region of peak soot loading and into the soot-oxidation region of this turbulent flame. These spectra are presently being analyzed to extract spatial profiles of temperature and O_2/N_2 ratio. A sample set of mean temperature and oxygen profiles obtained at a heights of $z/D =$ 134 and 175 are shown in Figure 8, with corresponding profiles of the rms fluctuations shown in Figure 9. Peak soot volume loading is reached at $z/D = 134$, where a peak mean temperature near $T = 1700$ K is observed near $r = \pm 15$ mm ($r/D = 4.7$). By $z/D = 175$, the flame tip has closed, with the peak temperature now observed along the jet centerline. Turbulent fluctuations of both temperature and oxygen are observed to peak at a radial location of 35 mm, or $r/D \sim 10$ throughout this region of the flame.

Comparison of the CARS measurements to the ODT predictions is made in Figure 10, where a scatter plot is constructed from all instantaneous temperature/oxygen realizations. Single-laser-shot CARS measurements at $z/D = 175$ sampled at radial locations near the jet centerline, $r/D = -5$ to 5, are plotted for both hot- and cold-channel detection. Instantaneous ODT realizations are plotted alongside the measurements, and were sampled from all radial locations, as little variation in the scatter-plot behavior was observed with radial position. Conditionally averaged temperatures were computed by binning the temperature based on their O_2/N_2 value. Conditioned temperatures from the ODT simulations are within 1−2% of the CARS-measured values across a wide range of O_2/N_2 ratio. At low values of O_2/N_2, the measured temperatures fall below the simulated values. This disagreement is largely a result of the oxygen detection limit in the CARS measurements, which appears to occur near $O_2/N_2 = 0.03$ in the present data set. Below this detection limit the measured temperatures are statistically uncorrelated with oxygen, and all samples with little or zero ("rich" side conditions) O_2 in the CARS measurement volume are appear in the cluster of data points for $O_2/N_2 < 0.3$.
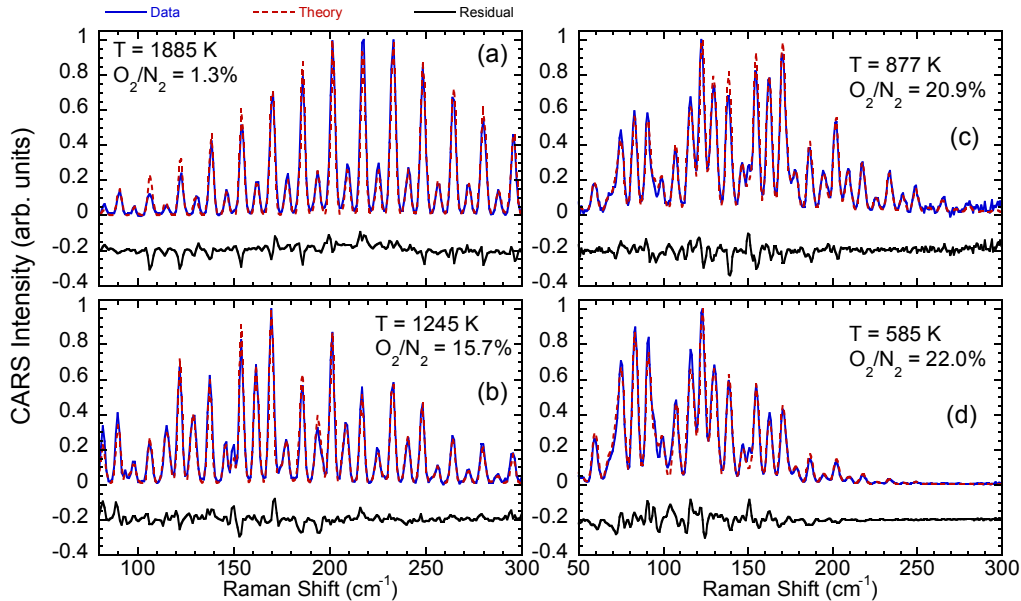
Figure 7. Single-laser-shot hybrid fs/ps rotational CARS spectra obtained at a height of $z/D = 175$ along the radial centerline of the jet flame. Results from the hot-channel are shown at left in (a,b) while spectra from the cold-channel are shown at right in (c,d).

Figure 8. Radial profiles of mean temperature and O_2/N_2 fluctuations at heights of z/D = 134 (upper) and z/D = 175 (lower). Temperature data are indicated by blue circles, while O_2/N_2 ratio data are shown as red triangles.

Figure 9. Radial profiles of rms temperature and O2/N2 fluctuations at heights of z/D = 134 (upper) and z/D = 175 (lower). Temperature data are indicated by blue circles, while O$_2$/N$_2$ ratio data are shown as red triangles.
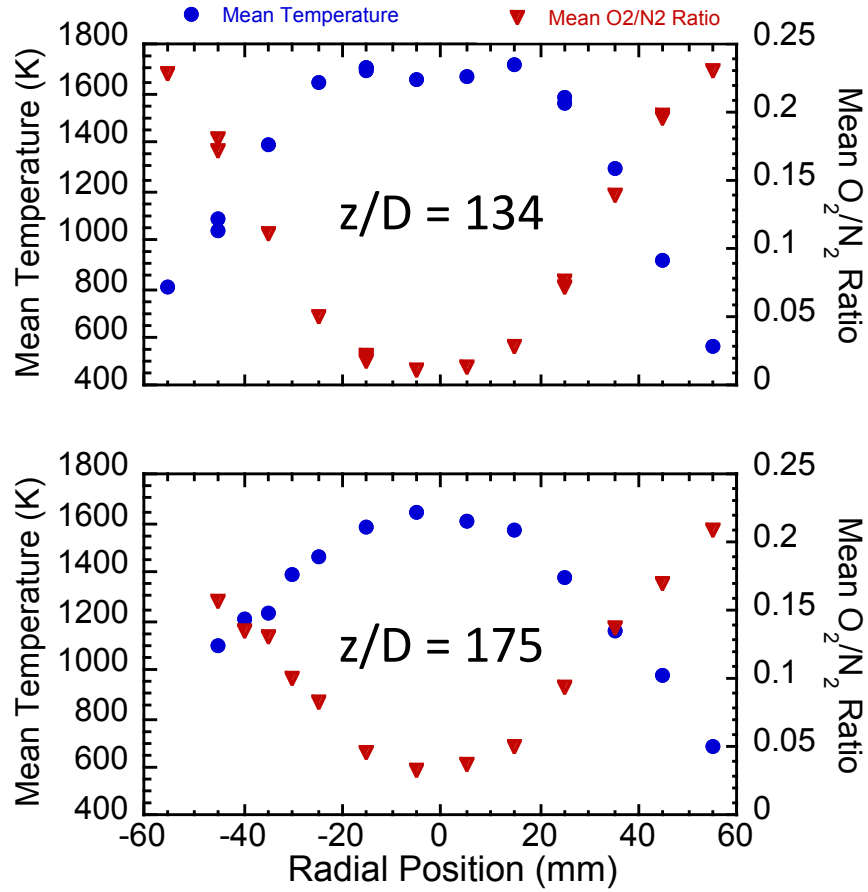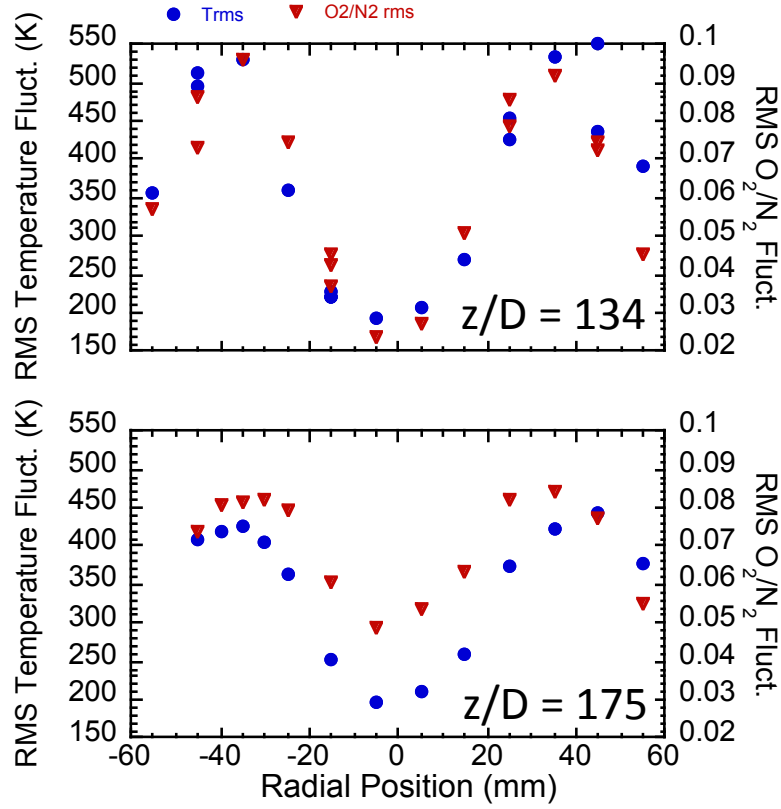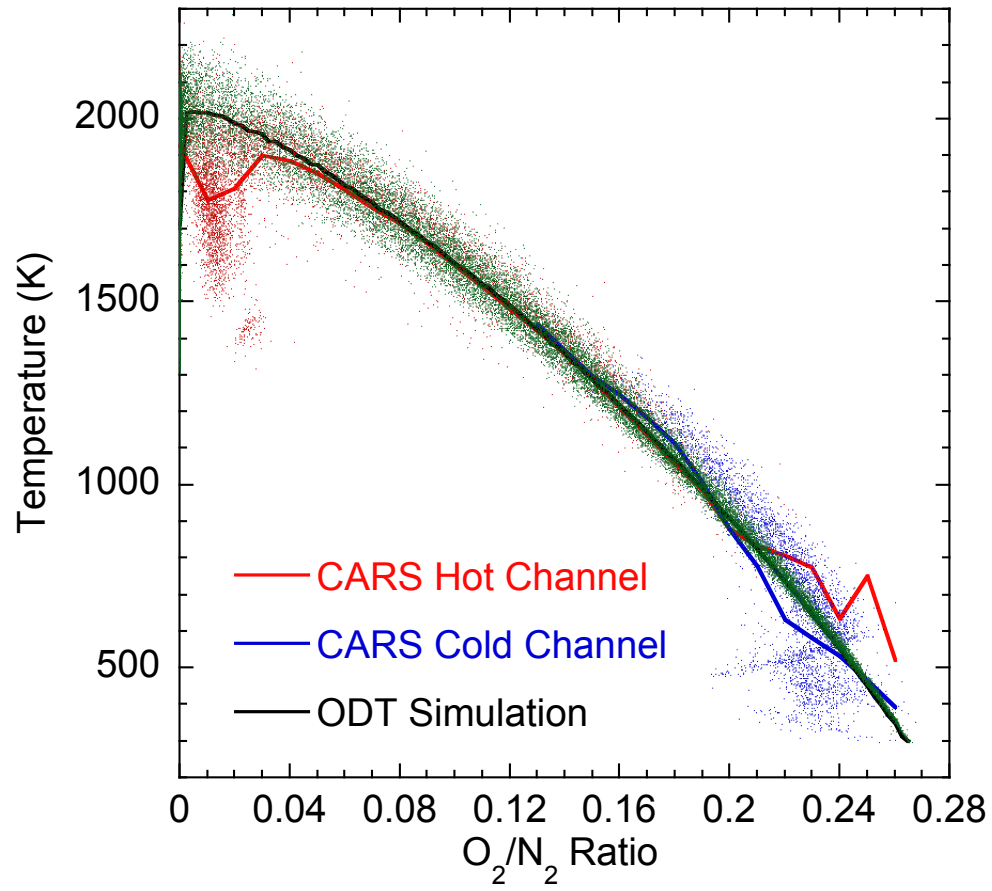
Figure 10. Comparison between fs/ps CARS measurements and ODT simulations: scatter plots and mean temperatures conditioned on O_2/N_2 ratio. Results are for a height of z/D = 175.

4. SUMMARY, CONCLUSION AND PATH FORWARD

High-fidelity laser diagnostics have been used to probe a sooting turbulent jet flame environment. Ultrafast CARS has been successfully implemented with enhanced dynamic range, using a two-channel detection system implemented specially for this application. LII measurements of soot were additionally conducted and the LII data from the soot growth region have been used to tune soot source terms in ODT modeling of soot radiation and transport in this turbulent flame. Using this tuned soot-production model, the ODT model was able to predict the measured temperatures higher up in the flame, within the soot-oxidation region. ODT-predicted temperatures were within $1-2\%$ of CARS measurements across the bulk of the lean side of the mixture-fraction space.

Future measurements will include product species, such as CO_2 and H_2 to begin to test the fire modeling tools on the rich side of the mixture fraction space. We are additionally implementing a newly developed [14] CARS imaging technique to obtain two-dimensional images of the temperature field simultaneously with soot LII. This new approach will allow us to spatially overlap the CARS temperatures with soot fields of the type shown in Figure 5. These simultaneous measurements will permit us to generate joint temperature/soot statistics to adequately measure the RTE emission term in Eq. 1.

(this page has been intentionally left blank)

5. REFERENCES

1. J. C. Hewson, D. O. Lignell, S. P. Kearney, D. R. Guildenbecher, and V. Lasinger, "One-dimensional turbulence simulation of soot and enthalpy evolution in ethylene jet diffusion flames," *Ninth U.S. National Combustion Meeting,* Combustion Institute, Cincinnati, OH, 2015.

2. A. L. Brundage, A.B. Donaldson, W. Gill, S.P. Kearney, V.F. Nicolette, N. Yilmaz, " Thermocouple Response in Fires, Part 1: Considerations in Flame Temperature Measurement by a Thermocouple," Journal of Fire Science*s* **29***,* 195-211 (2011).

3. F. Beyrau, T. Seeger, A. Malarski, and A. Leipertz, "Determination of Temperatures and Fuel/Air Ratios in an Ethene-Air Flame by Dual-Pump CARS," Journal of Raman Spectroscopy **34**, 946-951 (2003).

4. S. M. Mahmoud, G. J. Nathan, P. R. Medwell, B. B. Dally, and Z. T. Alwahabi, "Simultaneous planar measurement of temperature and soot volume fraction in a turbulent non-premixed jet flame," Proccedings of the Combustion Institute **35**, 1931-1938 (2015).

5. S. P. Kearney, K. Frederickson, and T. W. Grasser, "Dual-Pump Coherent Anti-Stokes Raman Scattering Thermometry in a Sooting Turbulent Pool Fire," Proceedings of the Combustion Institute **32**, 871-878 (2009).

6. K. Frederickson, S. P. Kearney, A. Luketa, J. C. Hewson, and T. W. Grasser, "Dual-Pump CARS Measurements of Temperature and Oxygen in a Turbulent Methanol-Fueled Pool Fire," Combustion Science and Technology **182**, 941-959 (2010).

7. K. Frederickson, S. P. Kearney, and T. W. Grasser, "Laser-induced incandescence measurements of soot in turbulent pool fires," Applied Optics **50**, A49-A59 (2011).

8. S. P. Kearney, and F. Pierce, "Evidence of soot superaggregates in a turbulent pool fire," Combustion and Flame **159**, 3191-3198 (2012).

9. J. Zhang, C. R. Shaddix, and R. W. Schefer, "Design of "model-friendly" turbulent non-premixed jet burners for C_2+ hydrocarbon fuels," Review of Scientific Instruments **82**, 074101 (2011).

10. C. R. Shaddix, J. Zhang, R. W. Schefer, J. Doom, J. C. Oefelein, S. Kook, L. M. Pickett, and H. Wang, "Understanding and predicting soot generation in turbulent non-premixed jet flames," (2010).

11. S. P. Kearney, "Hybrid fs/ps rotational CARS temperature and oxygen measurements in the product gases of canonical flat flames," Combustion and Flame **162**, 1748-1758 (2015).

12. A. C. Eckbreth, "BOXCARS: Crossed-Beam Phase Matched CARS Generation in Gases," Applied Physics Letters **32**, 421-423 (1978).

13. R. J. Santoro, and C. R. Shaddix, "Laser-Induced Incandescence," in *Applied Combustion Diagnostics*, K. K. Hoinghaus, and J. B. Jeffries, eds. (Taylor and Francis, 2002), pp. 252-286.

14. A. Bohlin, and C. J. Kliewer, "Diagnostic imaging in flames with instantaneous planar coherent Raman spectroscopy," The Journal of Physical Chemistry Letters **5**, 1242-1248 (2014).

DISTRIBUTION

(all copies distributed electronically)

1   The Ohio State University
    Attn: C. Winters
    Department of Mechanical Engineering
    Columbus, OH 43202

1	MS0815	J.E. Johannes	1500
1	MS0826	P.A. Farias	1512
1	MS0826	T.W. Grasser	1512
1	MS0826	S.P. Kearney	1512
1	MS0828	B. Hassan	1510
1	MS0828	T.L. Durbin	1512
1	MS0828	K.N.G. Hoffmeister	1512
1	MS0836	J.C. Hewson	1532
1	MS0840	D.R. Guildenbecher	1512
1	MS1135	A. Brown	1532
1	MS1135	R.D. Watkins	1532
1	MS0899	Technical Library	9536 (electronic copy)